Flow stability in a wide vaneless diffuser

S. Guadagni [a,*], M. Giachi [b], L. Fusi [a], A. Farina [a]

[a] Universitá degli Studi di Firenze, Dipartimento di Matematica e Informatica "U. Dini" Viale Morgagni 67/A, 50121 Firenze, Italy
[b] Baker Hughes Via Matteucci 2, Firenze, Italy

A B S T R A C T

This work is concerned with the theoretical aspects of flow stability in a two dimensional vaneless diffuser. Specifically, the appearance of self-excited oscillations, also referred to as rotating stall, is investigated considering a two-dimensional inviscid flow in an annulus. We consider a linear perturbation method, taking as basic flow the steady potential velocity field whose radial and tangential components are inversely proportional to the radial coordinate. We show that such flow may become unstable to small two-dimensional perturbations provided that the ratio between the inlet tangential velocity and the radial one is sufficiently large and a certain amount of vorticity is injected in the flow field. Such an instability is purely kinematical, i.e. it does not involve any boundary layer effects, contrary to the classical hypothesis which ascribes the instability to a peculiar boundary layers interaction.

1. Introduction

Compressors are used in aircraft engines, industrial gas turbines and turbo-charged combustion engines as well as in chemical industries (Lakshminarayana, 1996; Ludtke, 2004; Pfleiderer, 1952; Shepard, 1956). In this work we focus on centrifugal compressors. In these devices the flow is compressed by exploiting the centrifugal force due to the tangential velocity impressed on the gas by the rotating impeller. The static pressure of the gas is further increased downstream the impeller by means of a flow passage with increasing area.

The main components of centrifugal compressors are inducer, impeller, diffuser and volute as shown in Fig. 1.

The gas enters the compressor in axial direction through the inducer. Then it is accelerated in the impeller (which rotates at constant angular velocity) and decelerates in the diffuser until it arrives in the volute. The entire behaviour of the machine is driven by the amount of flow at fixed rotating speed.

In the past years a lot of attention has been drawn on the study of airflow dynamic in turbomachinery, because a reduction of the inflow rate at constant rotational speed may cause instability phenomena, usually termed rotating stall (Japikse and Baines, 1997; 1998; Ludtke, 2004), that consist of flow oscillations in one or more different parts of the compressor.

Numerical models, developed since nineties, reveal that in vaneless radial diffusers a rotating instability occurs when a critical inlet flow angle is reached, i.e. when the inflow falls below a specific threshold depending on the device geometry. The presence of rotating stall affects the compressor performances inducing severe vibrations to the rotors. To this aim, it is fundamental to set up a reliable model which allows to predict the instability onset, i.e. the critical inflow angle. Indeed, the rotating stall is a key problem for achieving a good working range of a centrifugal compressor and a detailed understanding of the phenomenon is very important to anticipate and avoid it.

In the literature analytical, numerical and experimental approaches have been used to investigate rotating stall in vaneless radial diffusers. For example, Abdelhamid and Betrand (1980) and Abdelhamid (1983) studied the effects of the vaneless diffuser geometry on rotating stall. Frigne and Van den Braebussche (1984) made a distinction between different types of impeller and diffuser rotating stall in a centrifugal compressor with vaneless diffuser. In Jansen (1964) the appearance of self-excited oscillations of large amplitude is investigated both theoretically and experimentally. Kinoshita and Senoo (1985), Senoo et al. (1977), Dou (1991), Shin et al. (1998), Ferrara et al. (2004), Biliotti (2013), Heng et al. (2018) and Engeda (2001a), Engeda (2001b), Engeda (2002) have observed rotating stall by studying the flow phenomena within vaneless radial diffusers. We also refer the readers to Chen (2003) for a wide review on this subject. All studies have been translated in the so-called stall maps or stall lines. The stall curve usually splits the plane into two regions: one corresponding to stable regimes and the other corresponding to the critical one, i.e. to the one in which the rotating stall occurs. In Kinoshita and Senoo (1985) numerous stall diagrams are shown.

* Corresponding author.
E-mail addresses: simone.guadagni@unifi.it (S. Guadagni), marco.giachi@bhge.com (M. Giachi), lorenzo.fusi@unifi.it (L. Fusi), angiolo.farina@unifi.it (A. Farina).
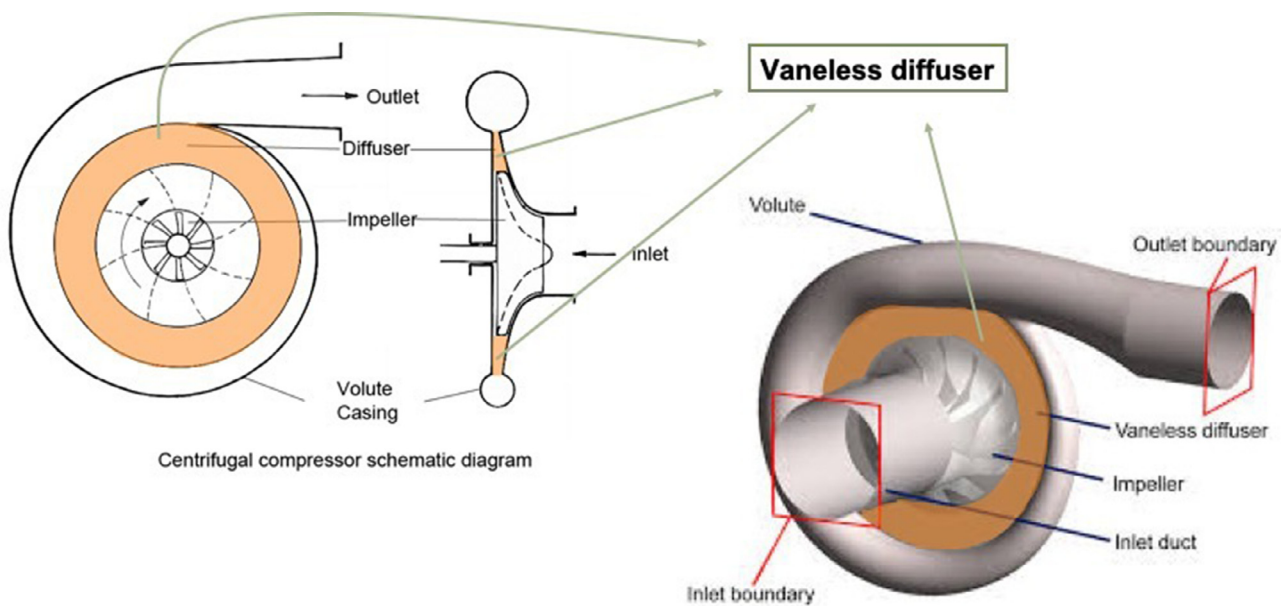
Fig. 1. A schematic of single stage a centrifugal compressor. Usually, centrifugal compressors are multi-stage, that is there are several impellers of different sizes that successively increase the gas pressure, bringing it to the intended level.

Historically, the stall instability has been explained by the occurrence of a reverse flow in a certain portion of the diffuser (Kobayashi et al., 1990). The presence of boundary layers on the top and bottom walls of the diffuser may cause the formation of a recirculation region, usually named recirculation bubble. According to Nishida et al. (1988), Kobayashi et al. (1990) when the bubble reaches a critical extension the instability is triggered. In other words, the rotating stall occurs when the radial velocity does not have sufficient "strength" to maintain the forward movement so to overcome the local adverse pressure gradient generated by the interaction between the boundary layers occurring on the diffuser upper and lower walls.

Recently, the problem of rotating stall has been analyzed with the support of CFD simulations. Thanks to such a new approach, it is believed that two or maybe more flow mechanisms might be responsible for the occurrence of rotating stall in vaneless diffusers. Indeed, measurements of Abdelhamid and Betrand (1980) have shown that wide vaneless diffusers behave differently from the narrow diffusers. Also Shin et al. (1998), Dou (1991) and Ljevar et al. (2005), Ljevar et al. (2006) clearly suggest that the vaneless diffuser performances also strongly depend on its width. These observations imply that a distinction should be made between narrow and wide vaneless diffusers. So two different flow mechanisms lead to the rotating stall instability. In general, one mechanism is associated with the flow instability occurring in wide vaneless diffusers; another mechanism causes the wall instability occurring in the narrow diffusers.

In wide diffusers the flow is essentially two-dimensional since the wall-boundary layers are well separated from each other. On the contrary, in narrow diffusers the wall-boundary layers merge before the flow comes out. In particular, in wide diffusers the instability has a kinematic origin, as we show in Section 3. Conversely, in narrow diffusers the instability originates from the interaction of the recirculation bubbles, which form on the upper and bottom diffuser walls.

The flow in a wide diffuser has some similarities with the one between two rotating concentric cylinders, and the circumferentially spaced stall cells in the diffuser are similar to the axially spaced convective cells occurring between rotating cylinders. Such a flow has been studied for many years from both theoretical and experimental points of view. We just recall the celebrated papers by Rayleigh (1880), Rayleigh (1917), Taylor (1923), the book by Chandrasekhar (1961) and the review by Howard (1962). However, the stability criteria concerning ro-

tating flow between cylinders refer only to tangential flows. In centrifugal compressors the flow has radial and tangential components. In this sense, a flow pattern similar to the one occurring in a diffuser is associated with the velocity field between two porous rotating cylinders Ilin and Morgulis (2013), Bellamy-Knights and Saci (1987). In a diffuser, however, there are no permeable boundaries. Indeed, while a boundary of the domain is clearly identifiable (that is the inlet), the other is missing. This is reflected in the selection of the peculiar boundary conditions that must be imposed.

The aim of this paper is to show theoretically that the inviscid rotationally invariant flow occurring in an annulus may become instable. More in detail, we consider, as basic steady flow, a velocity filed whose both components are inversely proportional to the radial coordinate. Next we perturb this basic flow with non-axisymmetric disturbances, i.e. with m azimuthal traveling vortices whose amplitude can grow or decrease in time. We show, analyzing the peculiar dispersion relation, that the basic inviscid flow is unstable to small two-dimensional perturbations provided that the ratio between azimuthal component of the velocity and the radial one is sufficiently large.

The paper develops as follows: In Section 2 we formulate the model. In Section 3 we describe the basic steady inviscid flow and formulate the linear stability problem. Section 4 is devoted to the analysis of the physical mechanisms that can trigger the instability. A comparison with the CFD data presented in Ljevar et al. (2005) is discussed in the last Section.

2. Mathematical model

We consider a flow in an annulus whose internal radius is[1] R_2^* and the external one is R_4^* (Fig. 2).

The velocity field is

$$\mathbf{v}^* = u^* \, \mathbf{e}_r + v^* \, \mathbf{e}_\theta,$$

where

$$u^* = u^* \left(r^*, \theta, t^* \right), \quad \text{and} \quad v^* = v^* \left(r^*, \theta, t^* \right), \tag{1}$$

$r^* \in [R_2^*, R_4^*]$ being the radial coordinate and $\theta \in [0, 2\pi)$ being the angular one. The fluid is injected into the annulus at the inner surface

---

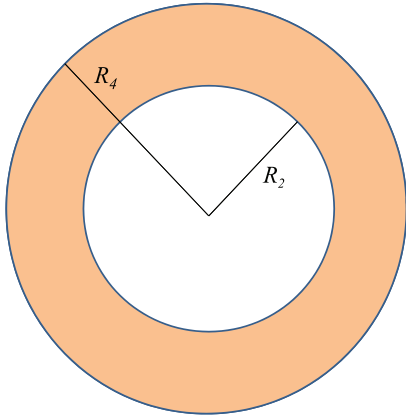[1] During the whole work we will mark with " * " the dimensional variables.

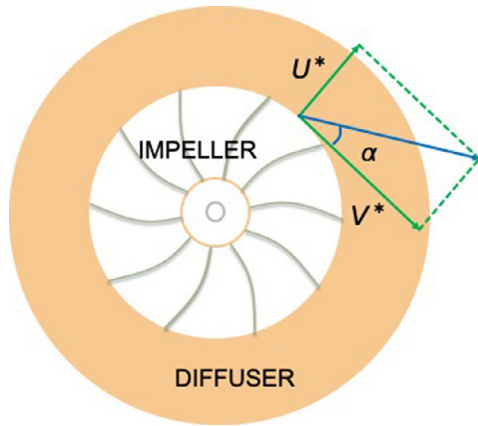**Fig. 2.** Annulus where the flow takes place. The typical are $R_2^* = 200$ mm, $R_4^* = 300$ mm.

Fig. 3. Schematic visualization of radial and tangential velocity, U^* and V^*, and the in between angle α.

$r^* = R_2^*$, where the radial and tangential velocity are prescribed[2]

$$u^*\big|_{r^*=R_2^*} = U^*(t^*) \geq 0, \tag{2}$$

$$v^*\big|_{r^*=R_2^*} = V^*(t^*) \geq 0. \tag{3}$$

We also introduce the angle α, as (see Fig. 4)

$$\alpha = arctan\left(\frac{U^*}{V^*}\right). \tag{4}$$

The vorticity is in the z direction (orthogonal to the plane of the flow), i.e.

$$\boldsymbol{\omega}^* = \nabla \wedge \mathbf{v}^* = \omega^*(r^*, \theta, t^*)\mathbf{e}_z \tag{5}$$

with

$$\omega^*(r^*, \theta, t^*) = \frac{1}{r^*}\left[\frac{\partial}{\partial r^*}(r^* v^*) - \frac{\partial u^*}{\partial \theta}\right]. \tag{6}$$

Typically the flow is in the range such that the mechanical incompressible assumption is fulfilled. Therefore we have

$$\nabla^* \cdot \mathbf{v}^* = 0. \tag{7}$$

Next, we assume that the fluid is inviscid, so that the motion equations reduce to Euler equations

$$\rho^*\left(\frac{\partial \mathbf{v}^*}{\partial t^*} + \mathbf{v}^* \cdot \nabla \mathbf{v}^*\right) = -\nabla^* p^*, \tag{8}$$

---

[2] Here we adopt the convention that $\mathbf{e}_\theta$ is oriented so that $\mathbf{v}^*|_{r^*=R_2^*} \cdot \mathbf{e}_\theta = v^*|_{r^*=R_2^*} \geq 0.$

with p^* pressure. Rewriting (7) and (8) in cylindrical geometry and assuming azimuthal symmetry, i.e. $u^* = u^*(r^*, t^*)$, $v^* = v^*(r^*, t^*)$ and $p^* = p^*(r^*, t^*)$, we have

$$\begin{cases} \dfrac{\partial(r^* u^*)}{\partial r^*} = 0, \\[2mm] \dfrac{\partial v^*}{\partial t^*} + \dfrac{u^*}{r^*}\left[\dfrac{\partial(v^* r^*)}{\partial r^*}\right] = 0, \\[2mm] \dfrac{\partial u^*}{\partial t^*} + u^*\dfrac{\partial u^*}{\partial r^*} - \dfrac{v^{*2}}{r^*} = -\dfrac{1}{\rho^*}\dfrac{\partial p^*}{\partial r^*}. \end{cases} \tag{9}$$

We now introduce the following dimensionless variables:

$$R_2 = \frac{R_2^*}{R_2^*} = 1, \quad R_4 = \frac{R_4^*}{R_2^*}, \quad r = \frac{r^*}{R_2^*} \in [1, R_4], \quad t = \frac{t^*}{\frac{R_2^*}{U_0^*}}.$$

For both radial and tangential velocity we use as a reference velocity[3] U_0^*, i.e. the order of magnitude of the inlet radial velocity. So we obtain

$$u = \frac{u^*}{U_0^*}, \quad v = \frac{v^*}{U_0^*},$$

and the boundary conditions (2), (3) become

$$\begin{cases} u|_{r=1} = U(t), \quad \text{with} \quad U(t) = \dfrac{U^*(t^*)}{U_0^*}, \\[2mm] v|_{r=1} = V(t), \quad \text{with} \quad V(t) = \dfrac{V^*(t^*)}{U_0^*}. \end{cases} \tag{10}$$

Concerning the pressure, we set

$$p = \frac{p^*}{\rho^* U_o^{*2}}.$$

Now using dimensionless variables and the boundary condition $(10)_1$, Eq. $(9)_1$ can be easily solved getting

$$u(r, t) = \frac{U(t)}{r}. \tag{11}$$

while the tangential velocity is obtained solving a linear PDE of hyperbolic type. Next, recalling (6), Eq. $(9)_1$ entails

$$\frac{\partial v}{\partial t} + u\omega = 0, \tag{12}$$

where

$$\omega = \frac{1}{r}\frac{\partial(rv)}{\partial r} \tag{13}$$

is the dimensionless vorticity.

2.1. Stationary flow

We consider this inlet flow

$$U(t) = 1, \quad V(t) = V_0 = const.,$$

so that (11) rewrites as

$$u(r) = \frac{1}{r} \quad 1 \leq r \leq R_4, \tag{14}$$

while the azimuthal velocity is

$$v(r) = \frac{V_o}{r} \quad 1 \leq r \leq R_4, \tag{15}$$

which, because of (12), yields zero vorticity, ideed

$$\omega = \frac{1}{r}\frac{\partial V_0}{\partial r} = 0. \tag{16}$$

The pressure field is

$$p(r) = P(R_4) + \frac{(1 + V_o^2)}{2}\left(\frac{1}{r^2} - \frac{1}{R_4^2}\right) \quad 1 \leq r \leq R_4, \tag{17}$$

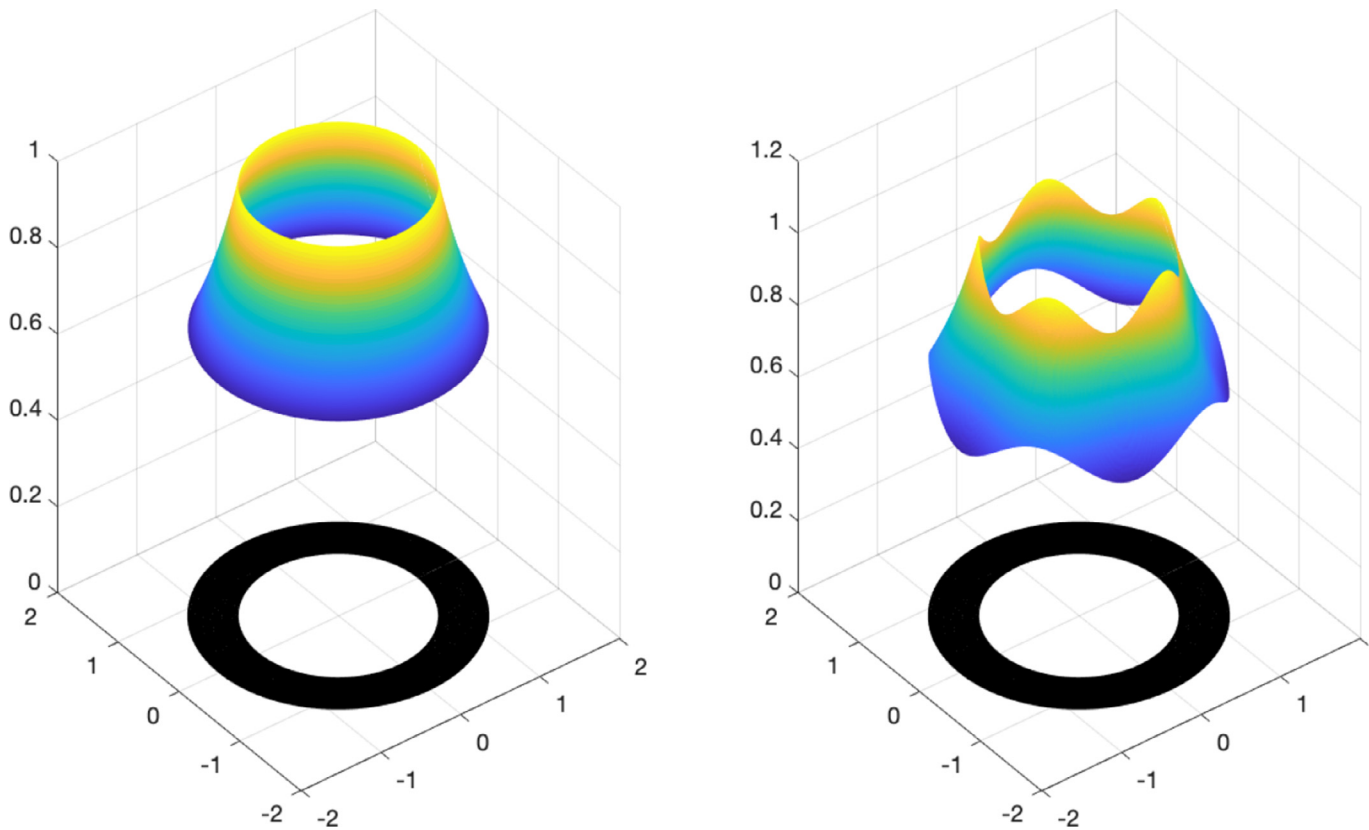[3] In diffusers the order of magnitude on the inlet radial and tangential velocities are similar.

Fig. 4. The stationary flow for the radial velocity field is shown on the left side, the perturbed one is shown on the right side.

so that the inlet-outlet pressure difference ΔP is

$$\Delta P = P|_{r=1} - P|_{r=R_4} = \frac{(1 + V_o^2)}{2}\left(1 - \frac{1}{R_4^2}\right). \tag{18}$$

3. Stability

The fluid enters the vaneless radial diffuser at the inner radius, $r = 1$, and flows outward at $r = R_4$. Self-excited oscillations may appear when the inlet angle α given by (4) goes under a threshold that, in turn, depends on R_4. We assume that the disturbances can be expressed in terms of periodic waves of small amplitude. The equations are then linearized and solutions are sought for the resulting characteristic value problem. More in detail, we add to the basic flow (14), (15) a small 2D perturbation and study the flow stability for every single mode.

We consider system (7) and (8), which we rewrite in a dimensionless form

$$\begin{cases} \dfrac{\partial(ru)}{\partial r} + \dfrac{\partial v}{\partial \theta} = 0, & 1 \leq r \leq R_4, \\[2mm] \dfrac{\partial v}{\partial t} + \dfrac{u}{r}\left[\dfrac{\partial(vr)}{\partial r}\right] + \dfrac{v}{r}\dfrac{\partial v}{\partial \theta} = -\dfrac{1}{r}\dfrac{\partial p}{\partial \theta}, & 1 \leq r \leq R_4, \\[2mm] \dfrac{\partial u}{\partial t} + u\dfrac{\partial u}{\partial r} - \dfrac{v^2}{r} + \dfrac{v}{r}\dfrac{\partial u}{\partial \theta} = -\dfrac{\partial p}{\partial r}, & 1 \leq r \leq R_4, \end{cases} \tag{19}$$

and take as basic flow (14), (15) and (17) where we have set $P(R_4) = 0$, i.e.

$$p(r) = \frac{1}{2}\left(1 + V_o^2\right)\left(\frac{1}{R_4^2} - \frac{1}{r^2}\right), \qquad 1 \leq r \leq R_4, \tag{20}$$

whose vorticity ω vanishes, as shown by (16). Next, we proceed as in Jansen (1964), considering[4]

$$\begin{cases} u = \dfrac{1}{r} + \hat{u}(r)e^{\sigma_R t}e^{i(\sigma_I t + m\theta)}, \\[2mm] v = \dfrac{V_o}{r} + \hat{v}(r)e^{\sigma_R t}e^{i(\sigma_I t + m\theta)}, \\[2mm] p = p(r) + \hat{p}(r)e^{\sigma_R t}e^{i(\sigma_I t + m\theta)}, \end{cases} \tag{21}$$

where $\sigma_R, \sigma_I \in \mathbb{R}$, $m \in \mathbb{N}$, and where the amplitude of the perturbations is estimated from $\hat{u}$, $\hat{v}$, $\hat{p}$, which are small. The perturbations represent azimuthal traveling waves, whose phase speed (or better angular phase speed) is $\dfrac{|\sigma_I|}{m}$ (see also Fig. 4). These rotating patterns are indeed the unsteady flows occurring in the vaneless diffuser, and the number of complete revolutions of these patterns per unit time is equal to $\sigma_I/2\pi$.

Setting

$$\sigma = \sigma_R + i\sigma_I,$$

and inserting (21) into system (19) and linearizing, we obtain the following system

$$\begin{cases} \left(\sigma + \dfrac{imV_o}{r^2} + \dfrac{1}{r}\dfrac{\partial}{\partial r}\right)\hat{u} - \dfrac{1}{r^2}\hat{u} - \dfrac{2V_o\hat{v}}{r^2} = -\dfrac{\partial\hat{p}}{\partial r}, & 1 \leq r \leq R_4, \\[2mm] \left(\sigma + \dfrac{imV_o}{r^2} + \dfrac{1}{r}\dfrac{\partial}{\partial r}\right)\hat{v} - \dfrac{\hat{v}}{r^2} = -\dfrac{im}{r}\hat{p}, & 1 \leq r \leq R_4, \\[2mm] \dfrac{\partial(r\hat{u})}{\partial r} + im\hat{v} = 0, & 1 \leq r \leq R_4. \end{cases} \tag{22}$$

---

[4] Here and in the sequel we use the exponential notation for the trigonometric functions, as implying that we are taking the real part
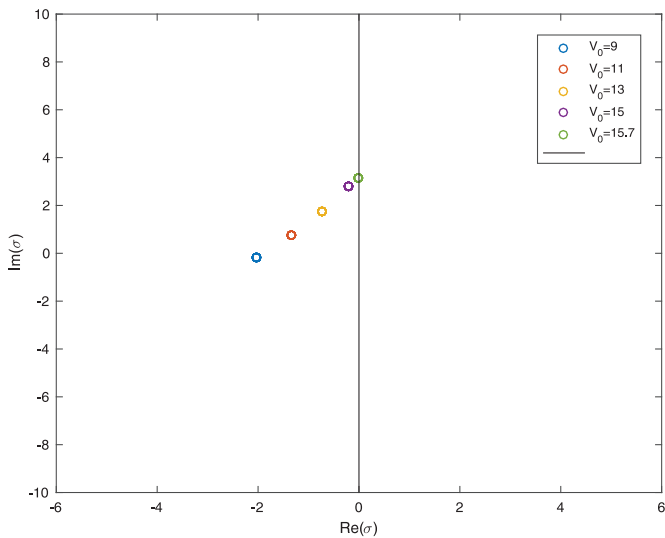
Fig. 5. Research of eigenvalue with $\sigma_R = 0$, for $m = 1$ and $R_4 = 1.5$.

Still following Jansen (1964), we introduce the stream function $\psi(r)$, since the flow is two-dimensional. Hence

$$\begin{cases} \hat{u} = \dfrac{im}{r}\psi(r), \\ \hat{v} = -\dfrac{\partial \psi(r)}{\partial r}, \end{cases}$$

so that the continuity Eq. $(22)_3$ is automatically fulfilled and, after some algebra, $(22)_{1,2}$ reduce to

$$\left(\sigma + \frac{imV_o}{r^2} + \frac{1}{r}\frac{\partial}{\partial r}\right)\nabla_r^2 \psi = 0, \tag{23}$$

where $\nabla_r^2(\cdot)$ is the radial part of the Laplacian in cylindrical coordinates, namely

$$\nabla_r^2(\cdot) = \frac{\partial^2(\cdot)}{\partial r^2} + \frac{1}{r}\frac{\partial(\cdot)}{\partial r} - \frac{m^2}{r^2}(\cdot). \tag{24}$$

We split (23) into the following system of two differential equations:

$$\begin{cases} \nabla_r^2(\psi) = f(r), \\ \left(\sigma + \dfrac{imV_o}{r^2} + \dfrac{1}{r}\dfrac{\partial}{\partial r}\right)f(r) = 0. \end{cases} \tag{25}$$

The solution to $(25)_2$ is

$$f(r) = c_3 e^{-g(r)}, \tag{26}$$

where

$$g(r) = \frac{\sigma(r^2 - 1)}{2} + imV_o \ln r,$$

with c_3 constant. Next, exploiting the variation of parameters method Boyce and DiPrima (2001), we solve $(25)_1$ getting this general solution

$$\psi(r) = \frac{c_1}{r^m} + c_2 r^m + \frac{c_3}{2m}\int_1^r (r^{-m}z^{m+1} - r^m z^{-m+1})e^{-g(z)}dz, \tag{27}$$

where c_1, c_2, (and c_3) are constants to be determined exploiting suitable boundary conditions. In particular, we impose $u_{r=1} = 1, \implies \hat{u}(r) = 0$, i.e.

$$\psi|_{r=1} = 0, \tag{28}$$

and $v|_{r=1} = V_0, \implies \hat{v}(r) = 0$, i.e.

$$\frac{\partial \psi}{\partial r}\bigg|_{r=1} = 0. \tag{29}$$

From the above conditions we easily obtain $c_1 = c_2 = 0$, but we still need a third boundary condition for the constant c_3. To this purpose, we have to bear in mind that R_4 is not a material boundary where the velocity can be prescribed. So on R_4 we can assign the pressure or, alternatively, we can prescribe the inlet-outlet pressure difference. We thus consider two possibilities:

- Prescribed outlet pressure,

$$p(R_4) = 0 \quad \underset{(21)_3}{\Rightarrow} \quad \hat{p}(R_4) = 0. \tag{30}$$

- Prescribed inlet-outlet pressure difference, namely

$$p(R_4) - p(1) = \Delta P \quad \underset{(21)_3}{\Rightarrow} \quad \hat{p}(R_4) - \hat{p}(1) = 0. \tag{31}$$

The procedure that we illustrate in the sequel refer to (30), but very minor changes allow to treat also (31). So, focussing on (30), we recast it in a condition for ψ, namely

$$\frac{\partial^2 \psi}{\partial r^2}\bigg|_{r=R_4} = -\left[\sigma R_4 + \frac{imV_o}{R_4} + \frac{1}{R_4}\right]\frac{\partial \psi}{\partial r}\bigg|_{r=R_4}. \tag{32}$$

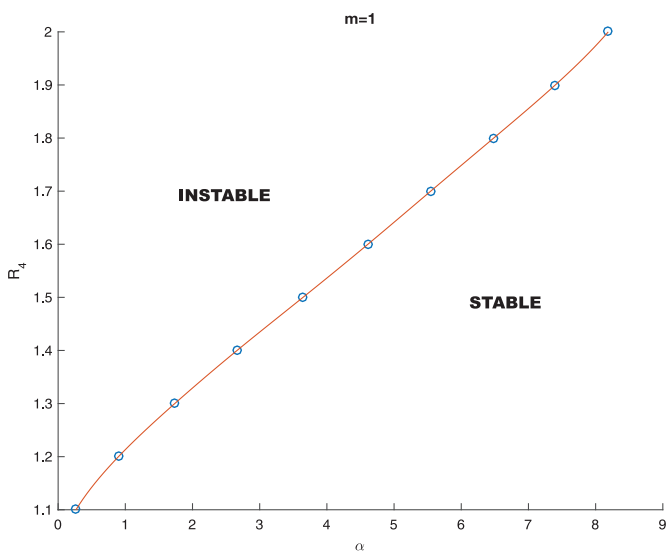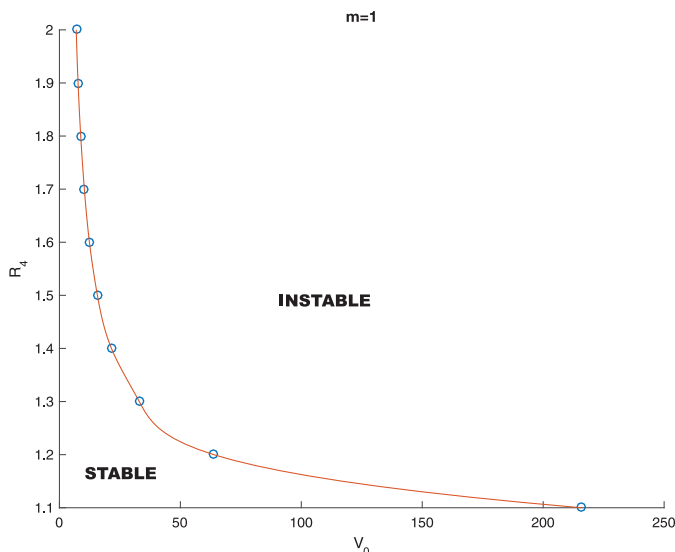If, in place of (30) we take (31), then Eq. (32) has to be replaced by

Fig. 6. Example of stall curve for $m = 1$. On the left the plane (V_o, R_4), on the right the plane (α, R_4), α being given by (4).
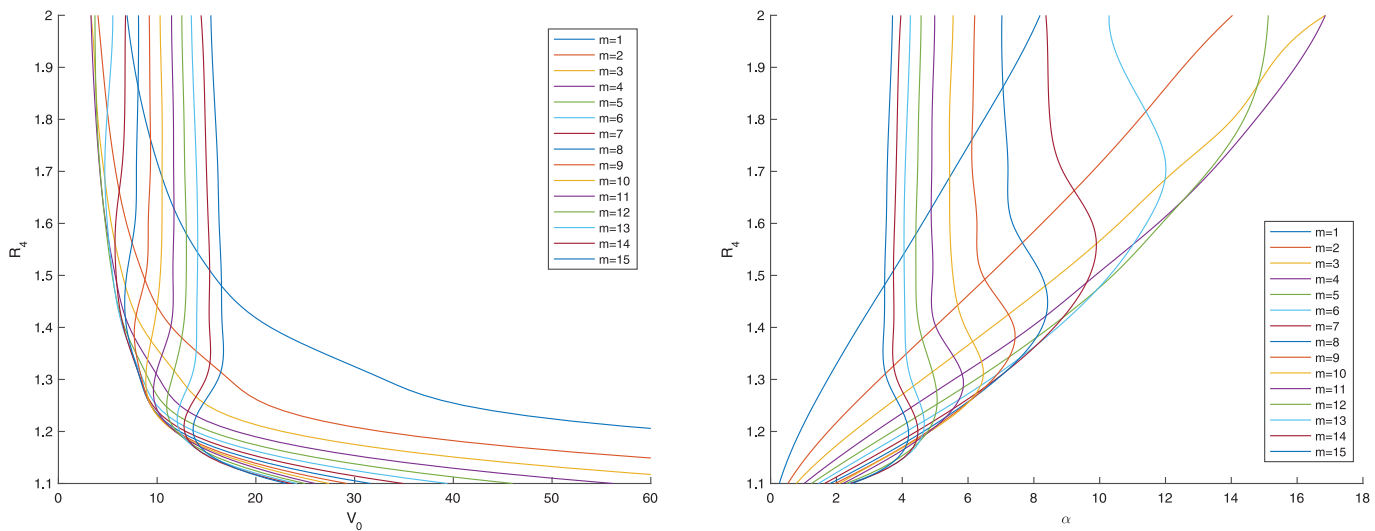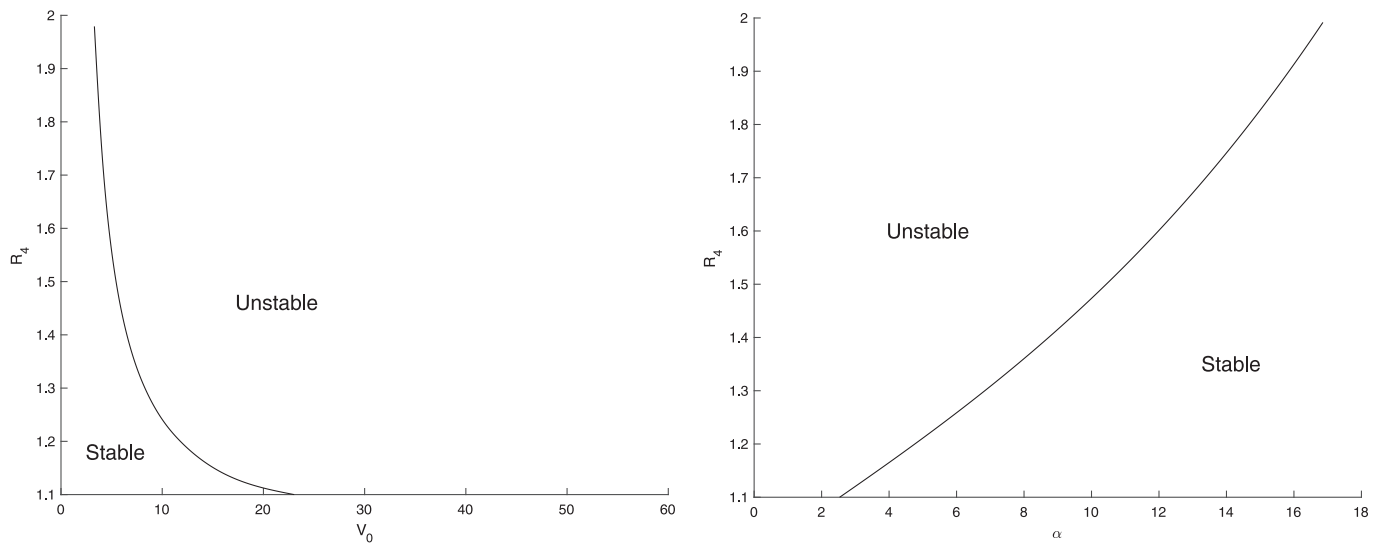
Fig. 7. Stall curves for $m = 1, ..., 15$.

Fig. 8. Stall curve obtained by composing the stall curves of the first 15 modes.

$$\left.\frac{\partial^2 \psi}{\partial r^2}\right|_{r=R_4} - \left.\frac{\partial^2 \psi}{\partial r^2}\right|_{r=1} + \left[\sigma R_4 + \frac{imV_o}{R_4} + \frac{1}{R_4}\right] \left.\frac{\partial \psi}{\partial r}\right|_{r=R_4}$$

$$- \left[\sigma + imV_o + 1\right] \left.\frac{\partial \psi}{\partial r}\right|_{r=1} = 0. \tag{33}$$

Recalling (27), Eq. (32), i.e. boundary condition (30), gives rise to such an equation

$$e^{-g(R_4)} = -\frac{1}{2} \int_1^{R_4} e^{-g(z)} \left\{ \left[mR_4^{m-2} z^{1-m} - mR_4^{-m-2} z^{1+m} \right] + \right.$$

$$\left. + \left[R_4^{m-2} z^{1-m} - R_4^{-m-2} z^{1+m} \right] (\sigma R_4^2 + imV_o) \right\} dz, \tag{34}$$

which, splitted into its real and imaginary parts, rewrites as

$$\begin{cases} 2e^E \cos(F) + \int_1^{R_4} (AC - BD) \, dz = 0, \\ 2e^E \sin(F) - \int_1^{R_4} (BC + AD) \, dz = 0, \end{cases} \tag{35}$$

where:

- $A = e^{-\frac{\sigma_R}{2}(z^2-1)} \cos\left(\frac{\sigma_I}{2}(z^2 - 1) + mV_o \ln(z)\right)$.
- $B = -e^{-\frac{\sigma_R}{2}(z^2-1)} \sin\left(\frac{\sigma_I}{2}(z^2 - 1) + mV_o \ln(z)\right)$.
- $C = R_4^{m-2} z^{1-m}(m + \sigma_R R_4^2) + R_4^{-m-2} z^{1+m}(-m + \sigma_R R_4^2)$.
- $D = (mV_o + \sigma_I R_4^2)(R_4^{m-2} z^{1-m} - R_4^{-m-2} z^{1+m})$.
- $E = -\frac{\sigma_R}{2}(R_4^2 - 1)$.
- $F = \frac{\sigma_I}{2}(R_4^2 - 1) + mV_o \ln(R_4)$.

So, (35) is a non-linear algebraic system in the variables σ_R and σ_I, usually named dispersion relation. The set of all (σ_R, σ_I) solution to system (35) gives the spectrum of the linearized problem.

To solve numerically (35) we impose a restriction on the range of σ_I, assuming $\frac{|\sigma_I|}{m} = \mathcal{O}(1)$. As stated earlier, the perturbation is an azimuthal travelling wave whose physical origin is essentially due to the impeller rotation. Hence, the perturbation angular phase speed, $\frac{|\sigma_I|}{m}$, has to be of the same order of the impeller angular velocity, which is 1 in dimensionless variables. In other words, the restriction $\frac{|\sigma_I|}{m} = \mathcal{O}(1)$, is due to the physical consistency of the model. We shall resume this issue on Section 4.
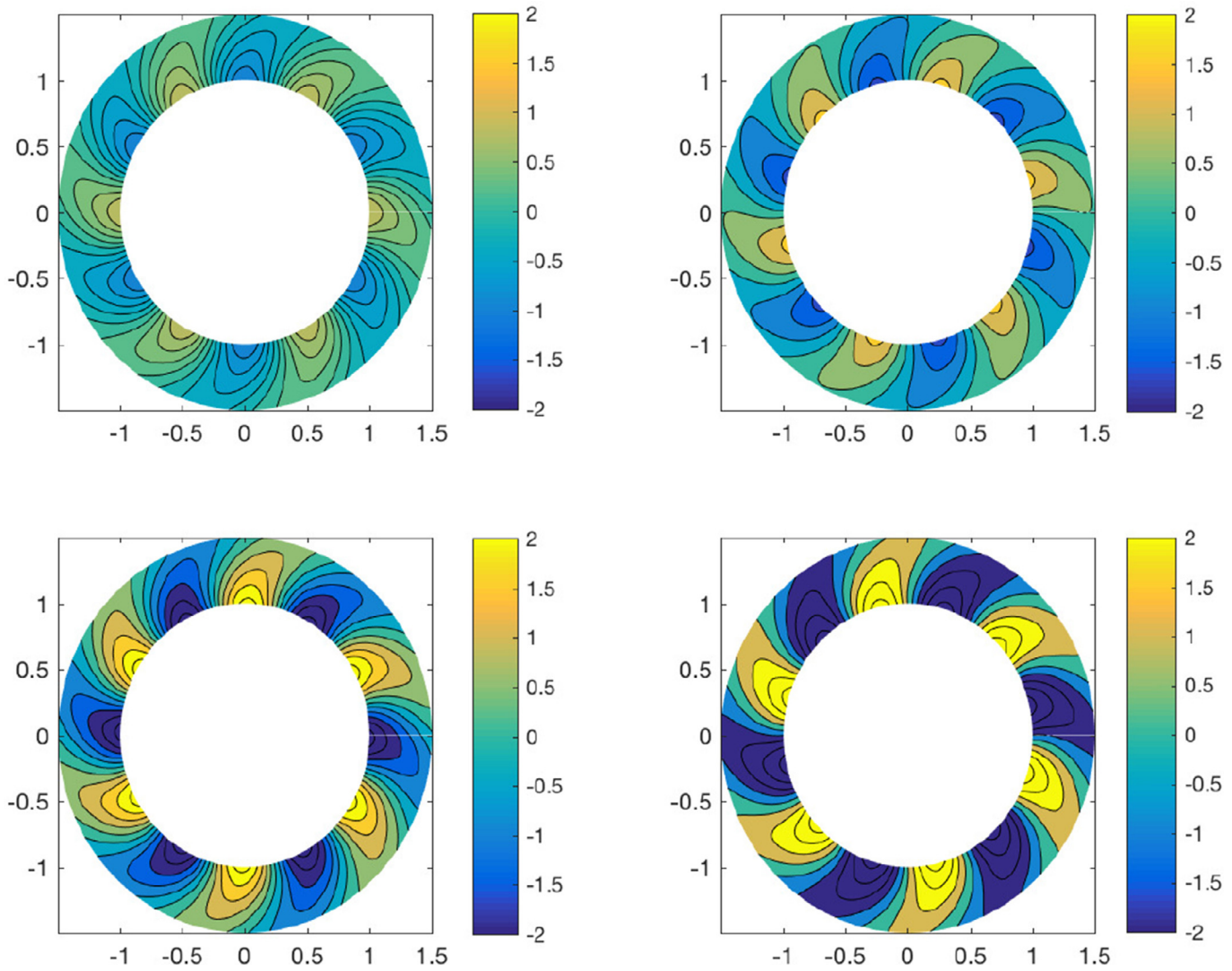
Fig. 9. Contour plot of the vorticity, for $m = 6$, $V_o = 1$, $\sigma_R = 2$ and $\sigma_I = 6$ for $t \in [0, \frac{2\pi}{\sigma_I}]$, $t = 0$, $\frac{\pi}{2\sigma_I}$, $\frac{\pi}{\sigma_I}$, $\frac{3}{2} \frac{\pi}{\sigma_I}$.

In solving numerically system (35) we are interested in those eigenvalues whose real part is positive. So, for given m and R_4 we look for the value of α for which σ_R becomes positive (see Chorin and Marsden (2000) Section 2.4). We repeat this procedure for $m = 1, 2, ..., 15$, and R_4 ranging in the interval (1.3, 2).

Numerical simulations indeed show that the purely radial flow (i.e. $\alpha = \pi/2$, or $V_o = 0$) is stable, i.e. $\sigma_R < 0$ for all $m \in [1, 15]$. When α is decreasing form $\pi/2$ (i.e. V_o is increasing from 0) the eigenvalues σ move to the right until σ crosses the imaginary axis, so σ_R becomes positive (see Fig. 5). The corresponding angle α has therefore reached a critical value at which the instability arises. So for each m we can draw in the (α, R_4) plane (or in the (V_0, R_4) plane) the neutral curve, i.e. the curve corresponding to $\sigma_R = 0$. Such a curve is therefore the stall curve relative to the m mode. In Fig. 6 we have plotted the stall curve for the mode $m = 1$.

Every stall curve splits the plane into two different regions: one corresponding to stable flow and the other corresponding to unstable flow. So, drawing the same plot for $m = 1, 2, ..., 15$, we have a characterization of the plane (α, R_4), or (V_o, R_4), in terms of the flow stability, as shown in Fig. 7.

Next, cutting out the instability region for each mode we obtain a single curve characterizing the flow stability/instability up to mode $m = 15$ (see Fig. 8).

So, on one side of the stall curve there is at least one mode $m \in [1, 15]$, which is unstable, i.e. which has at least one eigenvalue with $\sigma_R > 0$. On the other side of the stall curve all modes with $m \in [1, 15]$, have negative σ_R.

4. Instability onset: a possible explanation

Referring to the vorticity, form (21) we obtain

$$\omega = \hat{\omega}(r) \, e^{\sigma t + im\theta} = \underbrace{\frac{1}{r} \left[\frac{\partial}{\partial r}(r\hat{v}) - im\hat{u} \right]}_{\hat{\omega}(r)} \cdot e^{\sigma t + im\theta}. \tag{36}$$

Now recalling the stream function, we have $\hat{\omega}(r) = -\nabla_r^2 \psi$, so that

$$\omega(r, \theta, t) = -\left. \frac{\partial^2 \psi}{\partial r^2} \right|_{r=1} e^{\sigma\left(t - \frac{r^2-1}{2}\right) + im(\theta - V_o ln(r))},$$

whose real part is

$$Re(\omega) = -\left. \frac{\partial^2 \psi}{\partial r^2} \right|_{r=1} e^{\sigma_R\left(t - \frac{r^2-1}{2}\right)} \cos\left[\sigma_I\left(t - \frac{r^2-1}{2}\right) + m(\theta + V_o \ln(r))\right].$$

In particular,

$$\left. Re(\omega) \right|_{r=1} = -\left. \frac{\partial^2 \psi}{\partial r^2} \right|_{r=1} e^{\sigma_R t} \cos(\sigma_I t + m\theta),$$
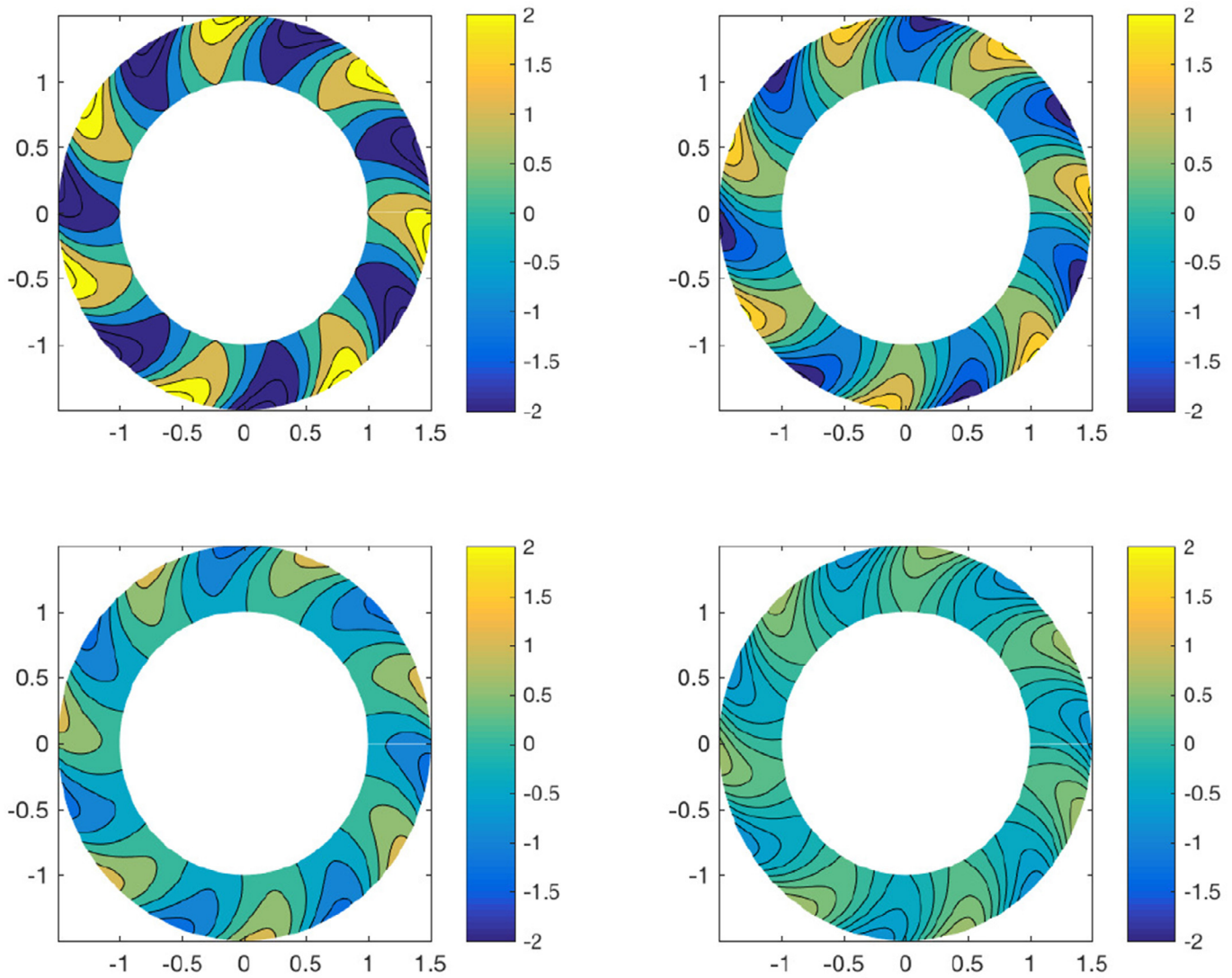
Fig. 10. Contour plot of the vorticity, for $m = 7$, $V_o = 1$, $\sigma_R = -2$ and $\sigma_I = 6$ for $t \in [0, \frac{2\pi}{\sigma_I}]$, $t = 0$, $\frac{\pi}{2\sigma_I}$, $\frac{\pi}{\sigma_I}$, $\frac{3}{2}\frac{\pi}{\sigma_I}$.
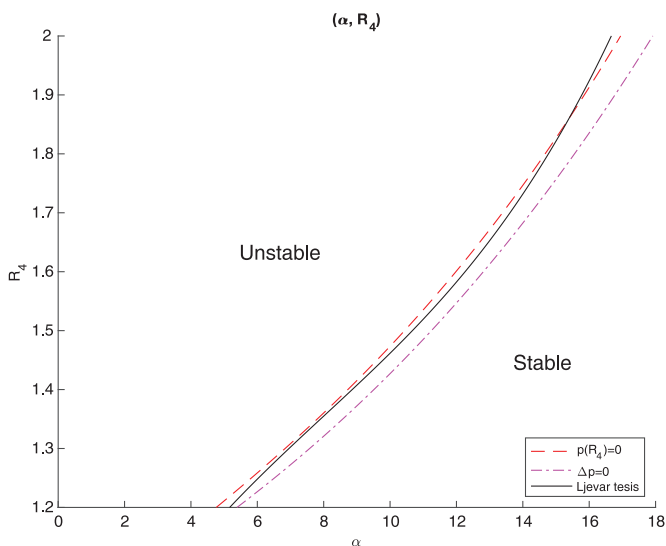

Fig. 11. Stall curves comparison.

showing that the perturbations generate a travelling circumferential wave in the vorticity at the inflow boundary, that then is advected across the annulus by the flow. We note that if we were to consider the flow with zero inlet vorticity, then instead of the boundary conditions (30) or (31), we should have considered the condition $\left.\frac{\partial^2 \psi}{\partial r^2}\right|_{r=1} = 0$, leading to the conclusion that the corresponding eigenvalue problem has no solution (and the flow is stable). So the instability may occur providing that $r = 1$ is not a zero-vorticity boundary. This fact gives an hint on the physical origin of the instability. The latter is likely to be generated by the wakes due to the rotating blades of the impeller. The vorticity that comes close to the blades (due to the fluid viscosity) is injected into the annulus essentially acting as a perturbation of the basic stationary flow (14), (15). When particular flow conditions occur, the injected vorticity is taken away by the mainstream, decreasing asymptotically. The resulting flow regime is thus stable. When such conditions are not fulfilled, the vorticity grows in time leading to the self-excited oscillations which persist inside the diffuser. Some plots of the vorticity for different values of σ_R are reported in Figs. 9 and 10.

To ascertain the validity of the proposed approach, we have reported in Fig. 11 the two stall curves, obtained by considering boundary conditions (30) and (31), and the stall curve obtained in

Ljevar et al. (2005) using a CFD approach based on a 2D inviscid model. The agreement is satisfactory.

5. Conclusions

The phenomenon of flow instability in centrifugal compressors is a long-standing problem of concern for turbomachinery research and application. It is well known indeed that the operating range of compression systems is limited at low mass flow rates by the onset of an instability. As the flow rate decreases, the pressure rise across the compressor increases monotonously until flow becomes unstable.

We address the problem from a linear stability point of view. Indeed, in the framework of the inviscid theory, we consider a simple irrotational flow resulting from a combination of source and vortex in an annulus to which we superimpose a small two-dimensional perturbations, without accounting for any boundary layers or other effects attributable to viscosity.

The analysis shows that basic flow (14), (15) becomes unstable when the ratio between the inlet velocity tangential and radial components exceeds a certain critical value (i.e. the inlet flow angle falls down a threshold value) provided that a certain amount of vorticity is injected in the flow field. Vorticity plays a fundamental role in the instability occurrence. The value of the critical flow angle at which the instability develops depends on the diffuser geometrical characteristic, in particular on the ratio between the external and internal radius.

This instability is purely kinematical. Indeed, the most unexpected result of this study is that such an instability develops in a 2D inviscid flow, while the classical results suggest that the instability origin lies in the fluid viscosity and in the thickness of the diffuser.

Much remains to be done in this area. One of the most interesting open questions is the stability of a three-dimensional flow, and, in particular, the relation with the two-dimensional case studied here. The results presented here, though mainly theoretical, are relevant to the above extent. They may also shed some light on the physical mechanism of the instability generation in narrow vaneless diffusers.

Declaration of Competing Interest

The authors declare that they have no known competing financial interests or personal relationships that could have appeared to influence the work reported in this paper.

Acknowledgments

References

Abdelhamid, A.N., 1983. Effects of vaneless diffuser geometry on flow instability in centrifugal compression systems. Can. Aeronaut. Space J. 29, 259–266.

Abdelhamid, A.N., Betrand, J., 1980. Distinctions between two types of self-excited gas oscillations in vaneless radial diffusers. Can. Aeronaut. Space J. 26, 105–117.

Bellamy-Knights, P.G., Saci, R., 1987. Viscous vortex core generation. Acta Mech. 67, 121–127.

Biliotti, D., 2013. Characterization of vaneless diffuser rotating stall on centrifugal compressors for industrial applications. School in Industrial Engineering, University of Florence Ph. D. thesis.

Boyce, W.E., DiPrima, R.C., 2001. Elementary Differential Equations and Boundary Value Problems. Wiley Interscience, New York.

Chandrasekhar, S., 1961. Hydrodynamic and Hydromagnetic Stability. Oxford University Press, Oxford.

Chen, J., 2003. - Flow instability and its control in compression systems. J. Therm. Sci. 12.

Chorin, A., Marsden, J., 2000. A Mathematical Introduction to Fluid Mechanics. Springer.

Dou, H.S., 1991. Investigation of the prediction of losses in radial vaneless diffusers. ASME Paper 91-GT-323, in Gas Turbine and Aeroengine Congress, Orlando 3-6 June, 1991, pp. 1–7.

Engeda, A., 2001. The unsteady performance of a centrifugal compressor with different diffusers. In: Proceedings of IMechE 2001, 215 (Part A), pp. 585–599.

Engeda, A., 2001. The unsteady performance of a centrifugal compressor with different diffusers: Part 1: Results of vaneless and conventional vaned diffuser. In: Proceedings of ASME Fluids Engineering Division Summer Meeting 2001, New Orleans, Louisiana, USA, 723-732.

Engeda, A., 2002. The influence of a diffuser width on the unsteady performance of a centrifugal compressor stage. In: Proceedings of ASME Fluids Engineering Division Summer Meeting 2002, Montreal, Quebec, Canada, pp. 1031–1041.

Ferrara, G., Ferrari, L., Baldassarre, L., 2004. Rotating stall in centrifugal compressor vaneless diffuser: experimental analysis of geometrical parameters influence on phenomenon evolution. Int. J. Rotat. Mach. 10, 433–442.

Frigne, P., Van den Braembussche, R., 1984. Distinction between different types of impeller and diffuser rotating stall in a centrifugal compressor with vaneless diffuser. ASME J. Eng. Gas Turbines Power 106, 468–474.

Heng, Y., Dazin, A., Ouarzazi, M.N., Si, Q., 2018. A study of rotating stall in a vaneless diffuser of radial flow pump. J. Hydraul. Res. doi:10.1080/00221686.2017.1399934.

Howard, L.N., 1962. Review of hydrodynamic and hydromagnetic stability by s. chandrasekhar. J. Fluid. Mech. 13, 158–160.

Ilin, K., Morgulis, A., 2013. Instability of an inviscid flow between porous cylinders with radial flow. J. Fluid Mech. 730, 364–378.

Jansen, W., 1964. Rotating stall in a radial vaneless diffuser. J. Basic Eng. 86 (4), 750–758.

Japikse, D., Baines, N.C., 1997. Introduction to Turbomachinery. Oxford University Press, Oxford.

Japikse, D., Baines, N.C., 1998. Diffuser design technology. Norwich, Concepts ETI, pp. 148–154.

Kinoshita, Y., Senoo, Y., 1985. Rotating stall induced in vaneless diffusers of very low specific speed centrifugal blowers. J. Eng. Gas Turbines Power 107, 514–521.

Kobayashi, H., Nishida, H., Takagi, T., Fukoshima, Y., 1990. A study on the rotating stall of centrifugal compressors (2nd report, effect of vaneless diffuser inlet shape on rotating stall). Trans. Jpn Soc. Mech. Eng. (B ed.) 56, 98–103.

Lakshminarayana, B., 1996. Fluid Dynamics and Heat Transfer of Turbomachinery. John Wiley & Sons Inc, New York.

Ljevar, S., de Lange, H.C., van Steenhoven, A.A., 2005. Rotating stall characteristics in a wide vaneless diffuser. In: Proceedings of the ASME Turbo Expo 2005, Reno-Tahoe, Nevada, USA.

Ljevar, S., de Lange, H.C., van Steenhoven, A.A., 2006. Two-dimensional rotating stall analysis in a wide vaneless diffuser. Int. J. Rotat. Mach. ID 56420, 1–11. 2006

Ludtke, K.H., 2004. Process Centrifugal Compressors. Springer-Verlag, Berlin Heidelberg.

Nishida, H., Kobayashi, H., Takagi, T., Fukoshima, Y., 1988. A study on the rotating stall of centrifugal compressors (1st report,effect of vaneless diffuser width on rotating stall). Trans. Jpn Soc. Mech. Eng. (B ed.) 54, 589–594.

Pfleiderer, C., 1952. Turbomachines. Springer-Verlag, New York.

Rayleigh, L., 1880. On the stability, or instability, of certain fluid motions. Proc. London Math. Soc. 11, 57–70.

Rayleigh, L., 1917. On the dynamics of revolving fluids. Proc. Royal Soc., Ser. A 93. No. 648, pp. 148–154.

Senoo, Y., Kinoshita, Y., Ishida, M., 1977. Asymmetric flow in vaneless diffuses of centrifugal blowers. Trans. ASME, J. Fluids Eng. 99, 104–111.

Shepard, D.G., 1956. Principles of Turbomachinery. McMillan.

Shin, Y.H., Kim, K.H., Son, B.J., 1998. An experimental study on the development of a reverse flow zone in a vanless diffuser. JSME Int. J. Ser. B 41, 546–555.

Taylor, G.I., 1923. Stability of a viscous liquid contained between two rotating cylinders. Philos. Trans. R. Sot. Lond, Ser. A 223, 289–343.